Long-range Cooper pair splitting by chiral Majorana edge states

Oscar Casas-Barrera,[1,2] Shirley Gómez Páez,[2] and William J. Herrera[2]
[1]Escuela de Física, Universidad Pedagógica y Tecnológica de Colombia, 150003 Tunja, Colombia
[2]Departamento de Física, Universidad Nacional de Colombia, 110911 Bogotá, Colombia

(Received 10 March 2023; revised 1 May 2024; accepted 21 June 2024; published 8 July 2024)

We analyze the transport properties of a Cooper pair splitter device composed of two-point electrodes in contact with a ferromagnetic/superconductor (F/S) junction constructed on the surface of a topological insulator (TI). For the pair potential in the S region, we consider s- and d-wave symmetries, while for the F region, we focus on a magnetization vector normal to the TI surface. Nonlocal transport along the F/S interface is mediated by chiral Majorana edge states, with chirality controlled by the polarization of the magnetization vector. We demonstrate that crossed Andreev reflections slowly decay with the separation of the electrodes in standard clean samples. Our system exhibits a maximum Cooper-pair-splitting efficiency of 80% for a symmetrical voltage configuration, even in high-temperature superconductor devices.

DOI: 10.1103/PhysRevB.110.045415

I. INTRODUCTION

In recent years, various solid-state systems with entangled electrons have been proposed for potential applications in quantum teleportation and computing [1]. Among these standout Cooper pair splitter devices, in which the electron pairs are stretched and extracted from the superconductor through nonlocal processes known as crossed Andreev reflections (CARs) [2–4]. The basic structure of such devices consists of a superconducting region (S) connected to two normal electrodes (N) separated by a distance of the order of the superconducting coherence length ξ_0 [2–32]. Various designs incorporate intermediate quantum dots [30,33–42] and anisotropic superconductivity [2,11,43–45], and indeed, some of these have been realized experimentally [14,15,17,19,24,35–37]. For subgap voltages, CARs compete with local Andreev reflections (AR) and elastic cotunneling (EC) between electrodes. Then, the pair-splitting efficiency is highly dependent on suppressing these secondary processes by appropriately setting the system parameters. While some systems could achieve an efficiency of 100% under ideal conditions, impurities or defects present in samples can lead to quantum noise and decoherence processes [46,47].

Topological superconductors (TSs) offer a potential solution to this problem by presenting surface Andreev bound states (SABSs) topologically protected against perturbations, preserving the discrete symmetries of the system [48–55]. Zero-energy SABSs are Majorana modes, quasiparticles that are their own antiparticle and exhibit nontrivial statistics. This characteristic makes them promising candidates for implementation in topological quantum computing devices [56–61]. Additionally, placing a conventional superconductor in contact with the surface of a topological insulator (TI) could give rise to an artificial chiral p-wave TS phase accompanied by chiral Majorana edge states (CMESs) at the interface with a magnetic domain or ferromagnetic region (F) [62–77].

In the last decade, several Cooper pair splitter devices on the surface of a TI have been proposed. Most of these are F/S/F planar junctions where exchange fields in the F regions influence the efficiency of CAR processes, their doping levels, interface transparency, or the pair potential symmetry (s or d) [78–82]. However, transport across interfaces in this configuration results in oscillating CAR conductance that decays rapidly over distances on the order of ξ_0 due to the mediation of evanescent states. Nevertheless, numerical calculations have revealed that the presence of a TS phase with chiral p-wave symmetry, as theorized for Sr_2RuO_4, may lead to nonlocal, unidirectional transport that is independent of the electrode spacing [83].

In this work, we investigate the spatial dependence and Cooper-pair-splitting efficiency of CMES-mediated CAR processes at the interface of an F/S planar junction on the surface of a TI. In the F region, the TI is in contact with a ferromagnetic insulator with a magnetization vector normal to the surface. In the S region, the TI is proximitized by an intrinsic s- or d-wave superconductor. For s symmetry, we observe that the CMESs lead to nonoscillating, long-range unidirectional CAR transport between the electrodes. This transport has a decay length of the order of $10^2\xi_0$ for samples with a typical number of impurities, similar to that found in [83]. However, in our system, the chirality can be controlled by the magnetization polarization of the F region, and the superconductivity is more robust against impurities compared to other potential chiral TSs like Sr_2RuO_4 [84,85]. In a Cooper pair splitter configuration, we suppress EC processes by applying symmetrical bias voltages to the electrodes, thereby achieving a maximum splitting efficiency of 80%. An analogous behavior is expected for $d_{x^2-y^2}$ symmetry; however, in this case, the samples must be exceptionally clean to avoid altering the superconducting state [86].

This article is structured as follows: Sec. II discusses the model of the system and contains a derivation of each region's Hamiltonian and transport observables. Section III examines a toy model with infinite magnetization, analyzes the dispersion relations of CMESs, and derives expressions for the conductance and the splitting efficiency as a function of the

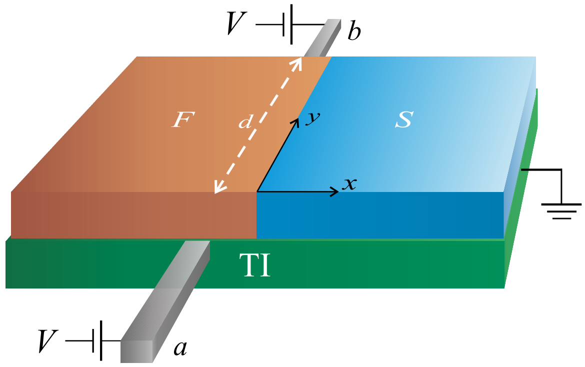

FIG. 1. Cooper pair splitter device consisting of an F/S junction on the surface of a TI and two metallic electrodes separated by a distance d. The F/S interface is formed through the proximity effect on the TI. CAR transport between electrodes is primarily mediated by the CMES at the F/S interface.

electrodes separation. Section IV presents the numerical calculations of observables for a system with finite magnetization and analyzes the dependence of CAR conductance on both the electrode separation and the magnetization value. Finally, Sec. V presents the conclusions of this work.

II. THEORETICAL FRAMEWORK AND TRANSPORT OBSERVABLES

The Cooper pair splitter device analyzed in this work is illustrated in Fig. 1. The system consists of an F/S planar junction constructed on the surface of a TI, in contact with two thin metallic electrodes. The F/S junction is formed through the proximity effect on the TI surface as follows: the left region is brought into contact with a ferromagnetic insulator (F), while the right region is brought into contact with a spin-singlet intrinsic superconductor (S), which can be either conventional (s wave) or high temperature (d wave). The two thin metal electrodes, denoted by a and b, are subjected to the same voltage bias V and are separated by a certain distance d on the TI surface within region F.

The elementary excitations of the superconducting state induced in the S region are described by the Bogoliubov–de Gennes (BdG) Hamiltonian [50,51,62,64,87,88]

$$\hat{H}_{\mathrm{BdG}} = \begin{pmatrix} \hat{H}_s & \hat{\Delta} \\ \hat{\Delta}^\dagger & -\hat{H}_s^\dagger \end{pmatrix}, \tag{1}$$

where $\hat{H}_s = v_F(\hat{\boldsymbol{\sigma}} \times \hat{\mathbf{p}})_z - E_F\hat{\sigma}_0$ is the effective Hamiltonian of the TI surface around the Γ point. Here, v_F represents the speed of the charge carriers at the Fermi level of the normal TI, $\hat{\mathbf{p}} = -i\hbar\nabla_{\mathbf{r}}$ is the momentum operator, $\hat{\boldsymbol{\sigma}} = (\hat{\sigma}_x, \hat{\sigma}_y, \hat{\sigma}_z)$ is the vector of Pauli matrices in the spin subspace, and $\hat{\sigma}_0$ is the corresponding identity matrix. E_F denotes the Fermi level of the system [89,90]. The induced superconducting order parameter is given by $\hat{\Delta} = \Delta_0 \cos[\beta(2\theta + \alpha)]i\hat{\sigma}_y$, where θ is the polar angular coordinate ($\beta = 0$ for s-wave symmetry, $\beta = 1$ for d-wave symmetry, $\alpha = 0$ for $d_{x^2-y^2}$, and $\alpha = \pi/2$ for d_{xy}). In the weak coupling limit ($E_F \gg \Delta_0$), the system's properties are predominantly determined by the states near the Fermi surface ($\hat{\psi}_e \simeq (1, -ie^{i\theta}, 0, 0)^T/\sqrt{2}$ and $\hat{\psi}_h \simeq (0, 0, -1, ie^{-i\theta})^T/\sqrt{2}$). When projecting $\hat{H}_{\mathrm{BdG}}$ onto this basis of states, we obtain the following effective spinless anisotropic order parameter with mixed symmetry:

$$\Delta_{\mathrm{eff}} = \langle\hat{\psi}_e|\hat{H}_{\mathrm{BdG}}|\hat{\psi}_h\rangle = i\Delta_0 \cos[\beta(2\theta + \alpha)]\mathrm{e}^{-i\theta}. \tag{2}$$

To describe the normal left region F with an induced exchange field perpendicular to the surface, $\mathbf{M} = M\hat{\mathbf{z}}$, we set $\hat{\Delta} = \hat{0}$ in (1) and introduce the corresponding Zeeman-type term $\hat{H}_Z = M\hat{\sigma}_z$ to the $\hat{H}_s$ Hamiltonian. This term breaks the time-reversal symmetry of (1) at the F/S interface, inducing topologically protected CMESs [62,63,65]. It will be assumed that $E_F = 0$ for region F to ensure that transport occurs only on the TI surface [65].

The transport properties of this kind of two-dimensional (2D) junction can be described using a Hamiltonian approach [91,92], where adjacent regions of the system are coupled through a tight-binding Hamiltonian (refer to Appendix A). The equilibrium Green's functions for each isolated region are derived analytically using the asymptotic solution method [73,93–95] (see Appendixes B to D for technical details). Then, the equilibrium Green's functions for the entire system are computed nonperturbatively in the hopping parameters by solving an algebraic Dyson equation with the equilibrium Green's functions of the regions. Finally, the system's transport properties are calculated in terms of the nonequilibrium (or Keldysh) Green's functions, which can be expressed in relation to their equilibrium counterparts under a stationary regime.

For low voltages ($eV \ll \Delta_0$), an electron incident on an electrode can either be reflected as a hole within the same electrode (AR process), transmitted as an electron to the second electrode (EC process), or reflected as a hole at the second electrode (CAR process), which corresponds to Cooper-pair-splitting under time reversal [2–4,26,36,41]. For a configuration with symmetrical voltages ($V_a = V_b = V$), only AR and CAR processes contribute to the current of the system (e.g., as evaluated at electrode a)

$$I_a = I_{\mathrm{AR},a} + I_{\mathrm{CAR}}, \tag{3}$$

where the contribution of AR processes to the current is given by

$$I_{\mathrm{AR},a} = \frac{2e}{h}\int R_{\mathrm{AR},a}(E)(n_{aN,e} - n_{aN,h})dE, \tag{4}$$

with $R_{\mathrm{AR},a}$ being the local Andreev reflection coefficient given by

$$R_{\mathrm{AR},a}(E) = \mathrm{Tr}\big(\hat{\Gamma}_{aN,e}\hat{G}^r_{aaS,eh}\hat{\Gamma}_{aN,h}\hat{G}^a_{aaS,eh}\big). \tag{5}$$

Here, $\hat{G}^{a(r)}_{aa'S}$ represents the advanced (retarded) equilibrium Green's function of the system, evaluated at the coordinates of the point contact electrodes inside the S region. $\hat{\Gamma}_{aN,\mu} = 2\pi[\hat{t}_a^\dagger\hat{\rho}_{aN}\hat{t}_a]_{\mu\mu}$ are the level width matrices, with $\mu = (e, h)$ being a Nambu index, $\hat{t}_a$ being the hopping matrix in spin space between electrode i and the F/S junction, and $\hat{\rho}_{aN} = -\mathrm{Im}(\hat{g}^r_{aN})/\pi$ being the density of states matrix of electrode a with the retarded (advanced) equilibrium Green's function $\hat{g}^{r(a)}_{aN}$; $n_{aN,e/h}(E) = f_a(E \mp eV_a)$ represents the corresponding Fermi-Dirac occupancy functions. On the other hand, the

CAR contribution to the current is given by

$$I_{\rm CAR} = \frac{2e}{h}\int T_{{\rm CAR},ab}(E)(n_{aN,e} - n_{bN,h})dE, \quad (6)$$

where the respective transmission coefficient $T_{{\rm CAR},ab}$ is given by

$$T_{{\rm CAR},ab}(E) = {\rm Tr}\big(\hat{\Gamma}_{aN,e}\hat{G}^r_{abS,eh}\hat{\Gamma}_{bN,h}\hat{G}^a_{baS,eh}\big). \quad (7)$$

Despite the formal resemblance of the last expressions to the more traditional Blonder Tinkham Klapwijk formalism, they are applicable beyond the tunnel limit approximation ($[\hat{t}_a]_{\sigma\sigma'} \ll \hbar v_F$) and involve all perturbation orders with respect to the hopping parameters between regions [91]. In our system, there is only competition between CAR and AR processes, which is reflected in the expression for the total differential conductance across electrode a ($\sigma_a = dI_a/dV$) at $T = 0$,

$$\sigma_a(V) = 2\sigma_0[T_{\rm CAR}(V) + T_{\rm CAR}(-V) + 2R_{{\rm AR},a}(V)], \quad (8)$$

where $\sigma_0 = 2e^2/h$ is the quantum of conductance and the Cooper-pair-splitting efficiency is defined as [26,36,41]

$$\eta = 4\sigma_0\frac{T_{\rm CAR}(V) + T_{\rm CAR}(-V)}{\sigma_a(V) + \sigma_b(V)}. \quad (9)$$

For η to be equal to 1, the local Andreev reflections are completely suppressed. It is convenient to compare the CAR conductance (8) with the electronic conductance of the system in its normal state and null magnetization for $d = 0$:

$$\sigma_{ee,0} = \sigma_0 T_{\rm EC}(0). \quad (10)$$

III. TOY MODEL

First, we consider the system depicted in Fig. 1 under conditions of high doping in the S region ($E_F \gg \Delta_0$, $k_{e/h} \simeq k_F$), high magnetization of the F region ($M \gg \Delta_0$), and the tunnel limit for the electrode couplings (refer to Appendixes B to D for further details). Under these conditions, the Green's function of the system, evaluated at the point contact of the electrodes with the F/S interface, is represented by (C15) with $x_a = x_b = 0$ and $y_b - y_a = d$, where the integrand $\hat{G}^{r,a}_{RR}(E, 0, 0, q) \simeq \hat{g}^{r,a}_{S0}(E, q)$ corresponds to the equilibrium Green's function of the uncoupled S region (B3),

$$\hat{g}^{r,a}_{S0}(E, q) = \frac{-1}{\hbar v_F}\begin{pmatrix} K & 0 & N{\rm e}^{-i\phi_+} & 0 \\ 1 & 0 & 0 & 0 \\ N{\rm e}^{i\phi_-} & 0 & K & 0 \\ 0 & 0 & -1 & 0 \end{pmatrix}, \quad (11)$$

with $q \simeq k_F \sin\theta$ being the conserved wave vector along the interface,

$$K = \frac{i}{D}\big(1 - \gamma_0^2{\rm e}^{-i\Delta\varphi}\big),\quad N = -\frac{\gamma_0}{D}({\rm e}^{i\theta} + {\rm e}^{-i\theta}),$$
$$D = {\rm e}^{i\theta} + \gamma_0^2{\rm e}^{-i\theta}{\rm e}^{-i\Delta\varphi}, \quad (12)$$

$$\gamma_0 = \sqrt{\frac{E-\Omega}{E+\Omega}},\quad \Omega = \sqrt{E^2 - \Delta(\theta)^2}. \quad (13)$$

For the case of a strong magnetic barrier, the dispersion relation of the SABS is obtained from the poles of the Green's function (11) and can be expressed as

$$E = \pm|\Delta_{\rm eff}|\cos(\Delta\varphi/2), \quad (14)$$

$$\Delta_+ = \Delta_{\rm eff}(\theta),\quad \Delta_- = \Delta_{\rm eff}(\pi - \theta),$$
$$\Delta\varphi = \varphi_+ - \varphi_-,\quad \varphi_\pm = \arg(\Delta_\pm), \quad (15)$$

where $\Delta_{\rm eff}$ is the effective surface gap given by (2). It is important to note that our model aligns with the general expression for SABSs [96] and is consistent with those found for planar F/S junctions in TIs with finite magnetizations [62,63,65]. In Fig. 2(a), CMES dispersion curves are shown for s-wave, $d_{x^2-y^2}$, and d_{xy} symmetries. These states are also depicted in Figs. 2(b) and 2(c), where the spectral density $A(q, E) = {\rm Tr}[\hat{\rho}_{F/S}(q, E)]$ evaluated at the interface of an F/S junction with infinite magnetization is shown for different symmetries of the pair potential.

The dispersion relation is linear in q for s-wave symmetry but undulated for d-wave symmetries. Note that the densities of states for both s-wave and $d_{x^2-y^2}$ symmetries present a

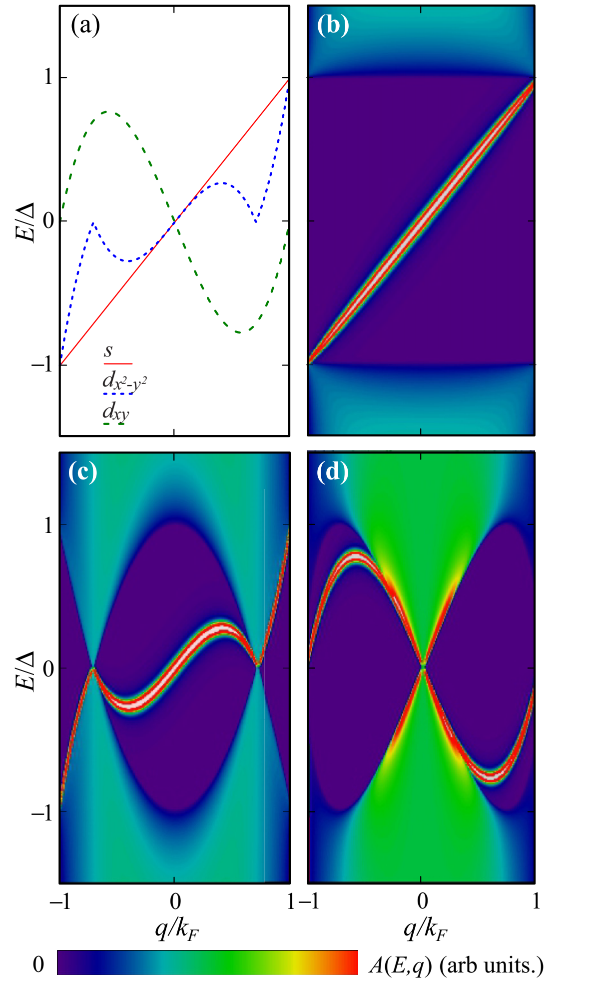

FIG. 2. (a) Surface Andreev bound states at the F/S interface with infinite magnetization obtained from expression (14) ($M \to -\infty$). The opposite polarization of M changes the function's parity. Spectral density A evaluated at the F/S junction interface for a superconductor with (b) s-wave, (c) $d_{x^2-y^2}$, and (d) d_{xy} symmetry. In all three cases, the presence of chiral Majorana edge states is observed.

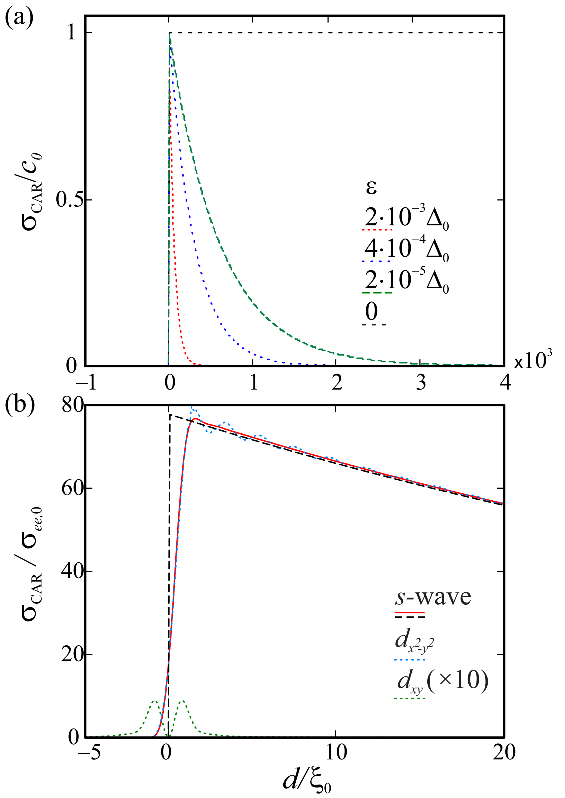

FIG. 3. (a) Crossed Andreev reflection conductance $\sigma_{\rm CAR}(V = 0)$ along the F/S interface as a function of distance d for s-wave symmetry with infinite magnetization (16), $E_F = 13\Delta_0$, and different values of ε in the tunnel limit. All curves in (a) are normalized to c_0 (17). (b) Curves of $\sigma_{\rm CAR}(V = 0)$ for the different symmetries with infinite magnetization, $E_F = 13\Delta_0$, and $\varepsilon = 0.002\ \Delta_0$. The dashed black line represents the fit with the analytic function (16) for s-wave symmetry. All curves in (b) are normalized to $\sigma_{ee,0}$ (10).

high value and have the same chirality near $q = 0$, while for d_{xy} it becomes symmetrical and diffuse. In all instances, the dispersion relations are odd functions of q, and the polarization of magnetization in the F region defines their chirality. The following section shows that these states account for the solid chiral character of nonlocal transport processes along the interface.

For s-wave symmetry and $V = 0$, the calculation of (7) can be performed analytically, resulting in

$$\sigma_{\rm CAR}(d) = c_0\left[\Theta(sd)\left(1 + \frac{\varepsilon}{\Delta_0}\right)\right]^2 {\rm e}^{-d/\lambda}, \tag{16}$$

$$c_0 = \sigma_0\tilde{\Gamma}_{e,b}\tilde{\Gamma}_{h,a}(2\pi iL/\hbar v_F)^2(k_F/\pi)^6, \tag{17}$$

where $\Theta(x)$ is the Heaviside step function, $s = -{\rm sgn}(M)$, $\tilde{\Gamma}_{\mu,iN} \equiv {\rm Tr}[\hat{\Gamma}_{\mu,iN}]$, ε is the imaginary part of the excitation energy, and $\lambda = \Delta_0/2\varepsilon k_F = \xi_0(\hbar v_F/2\pi\varepsilon k_F)$ represents the characteristic decay length of CAR processes along the interface. Here, $\xi_0 = \pi\Delta_0/\hbar v_F$ is the coherence length of the conventional superconductor. The curves in Fig. 3(a) show the behavior of $\sigma_{\rm CAR}(d)$ for different values of ε.

Note that the electron-hole component of the Green's function exhibits unidirectional behavior (odd with distance) and approaches the step function in the limit $\varepsilon \to 0$. Since $\varepsilon \sim \hbar/2\Delta\tau$, with $\Delta\tau$ representing the quasiparticle lifetime, it is expected that for weak-disorder junctions, these processes have a long range (decay length on the order of $10^2\xi_0$), similar to that observed in a 2D intrinsic p-wave chiral superconductor (Appendix E) or a three-dimensional one [83]. In this case, the propagating CMES present along the F/S interface favorably mediates the CAR processes and confers their chirality and topological protection. It is essential to highlight that this distance-dependent behavior contrasts with that obtained for conventional superconductors with s-wave $[\sigma_{\rm CAR}(d) \propto {\rm e}^{-2d/\pi\xi_0}/d^3]$ or d-wave $[\sigma_{\rm CAR}(d) \propto 1/d^2]$ superconductivity [44].

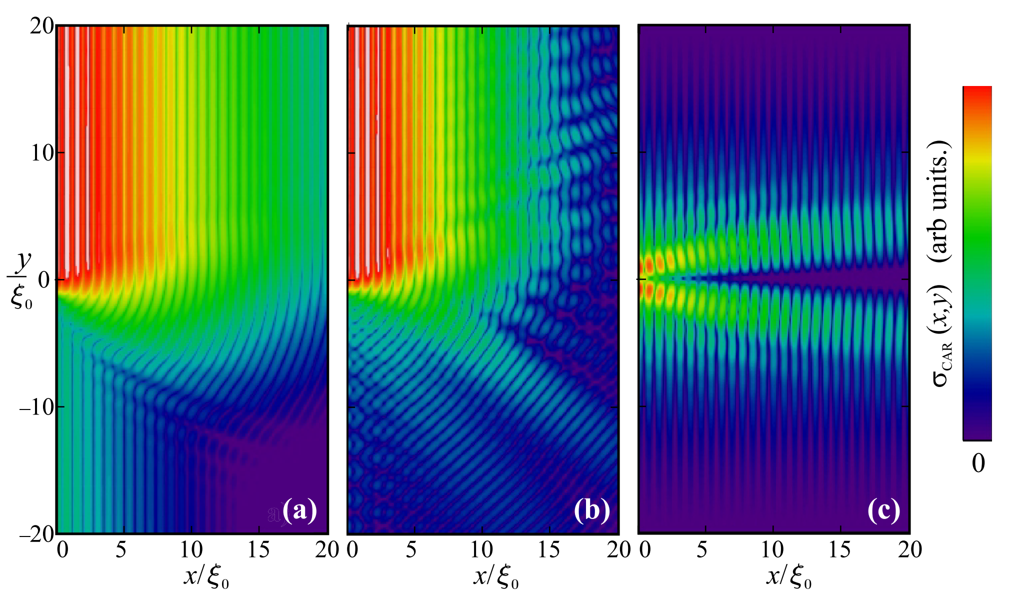

FIG. 4. Maps of crossed Andreev reflection conductance $\sigma_{\rm CAR}(V = 0)$ in the tunnel limit as a function of the b electrode coordinates over the S region with the a electrode fixed at the F/S interface $[\mathbf{r}_a = (0, 0), \mathbf{r}_b = (x, y)]$ for infinite magnetization of the F region and (a) s-wave, (b) $d_{x^2-y^2}$, and (c) d_{xy} symmetry for the S region. A logarithmic scale is used for $\sigma_{\rm CAR}$.

Although the conductance increases with the Fermi level of the S region, the direct AR conductance is approximately a quarter of that of the CAR. According to formula (9), the splitting efficiency percentage will reach a maximum of 80% for symmetrical voltages [$\Theta(0) = 1/2$]. In Fig. 3(b), the behavior of $\sigma_{\rm CAR}(V = 0)$ for infinite magnetization across different symmetries of the pair potential is observed. For the $d_{x^2-y^2}$ symmetry case, the results are qualitatively similar to those of the s-wave symmetry due to the mediation of CMESs around $q = 0$ [Fig. 2(c)] and because $\Delta\varphi = 0$ for most of the integration interval (except in the neighborhood of $\theta = \pm\pi/4$ nodes). However, there are slight additional oscillations due to the angular dependence of $\Delta(\theta)$. Both symmetries, s wave and $d_{x^2-y^2}$, closely align with the analytical result (16).

For the d_{xy} case, the overall amplitude is lower than in the previous cases. Here, $\sigma_{\rm CAR}(V = 0)$ is an even function of d with two small maxima flanking $d = 0$. This behavior is attributed to the presence of two low-density counterpropagating CMESs around $q = 0$ [Fig. 2(d)]. Mathematically, because $\Delta\varphi = \pi$ for the integration interval, D has real roots, and analytical integration is impossible. Furthermore, numerical computation shows an even behavior with distance, decreasing proportionally to $\sim 1/d^2$, as in the conventional d_{xy} case [44]. The mixed symmetry of the effective surface pair potential (2) and the corresponding nodal dispersion relation for SABSs with counterpropagating CMESs (14) [Fig. 2(d)] prevent the d_{xy} symmetry from presenting the characteristic zero bias conductance peak associated with the zero-energy flat SABS of the conventional d_{xy} case.

All these behaviors are also visualized in Fig. 4, where maps of $\sigma_{\rm CAR}(V = 0)$ are shown for the S region as a function of $\mathbf{r}_b$=(x, y), with $\mathbf{r}_a$ fixed at the F/S interface with infinite magnetization. As observed in Figs. 4(a) and 4(b) for s-wave and $d_{x^2-y^2}$ symmetries, respectively, the strong chirality of the nonlocal transport arises from the presence of CMESs around $\mathbf{k} = 0$. In contrast, for the d_{xy} case, a symmetrical interference pattern is observed due to the low spectral density of these states at $q = 0$.

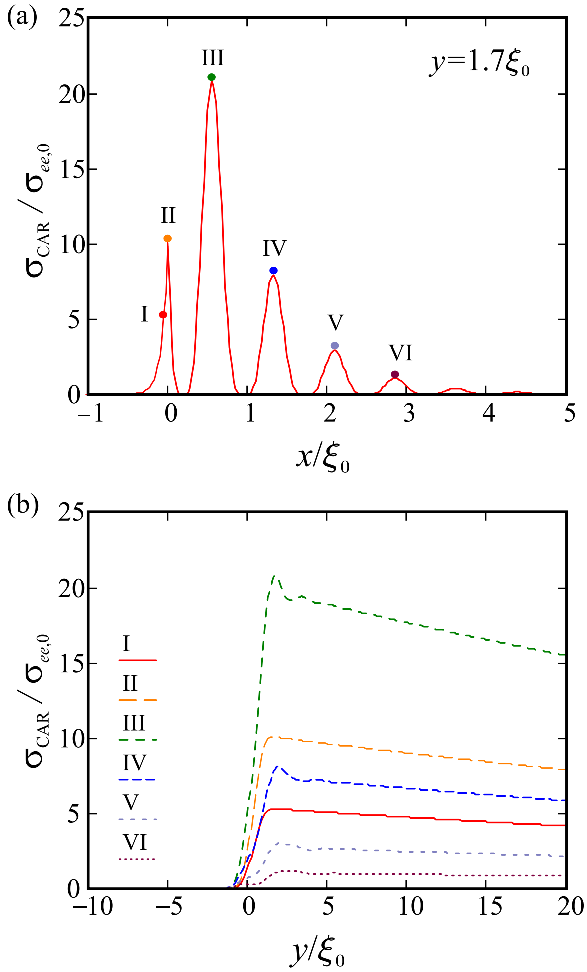

FIG. 5. Crossed Andreev reflection conductance $\sigma_{\rm CAR}(V = 0)$ for s-wave symmetry in the tunnel limit (a) as a function of the perpendicular distance to the interface F/S interface x for a constant electrode separation $d = y = 1.7\xi_0$ and (b) as a function of y for the points labeled in (a). In both panels, $M = -10\ \Delta_0$. All curves are normalized as in Fig. 3(b).

IV. COOPER PAIR SPLITTER DEVICE WITH FINITE MAGNETIZATION IN THE F REGION

In this section, we examine the system depicted in Fig. 1 with finite magnetization in region F. As shown in Fig. 5(a), $\sigma_{\rm CAR}$ exhibits an oscillatory decay towards the interior of region S over distances of approximately $5\xi_0$. In contrast, it decays smoothly towards region F ($x < 0$), with a characteristic length that decreases with the value of $|M|$. Across the interface, $\sigma_{\rm CAR}$ exhibits the behavior discussed above for the F/S interface for s-wave symmetry, as illustrated in Fig. 5(b), corresponding to the maxima in Fig. 5(a). The results for the s-wave symmetry show that the propagating CMESs facilitate long-range CAR transport along the F/S interface. Similarly, for the $d_{x^2-y^2}$ symmetry, analogous results were obtained despite the presence of nodes in $\Delta(\theta)$. This is because the longitudinal transport predominantly occurs along the lobes of $\Delta(\theta)$. This observation suggests the potential for achieving long-range CAR in high-temperature superconductors. In Fig. 6, we analyze the effect of the magnitude of $\mathbf{M}$ on the CAR conductance at the interface. Figure 6(a) displays the curves of $\sigma_{\rm CAR}(V = 0)$ for s-wave symmetry as a function of d for various magnetization values. As seen in Fig. 6(a), the maximum CAR conductance increases with the value of $|M|$, but at a decelerating rate until it reaches a limit value for $|M| = \infty$. A similar trend is observed for $d_{x^2-y^2}$ symmetry in Fig. 6(b), but with the same undulations as in Fig. 3. Another important aspect is that the decay length of $\sigma_{\rm CAR}$ decreases with magnetization until it reaches the minimum value of $\lambda = \Delta_0/2\varepsilon k_F$ for the infinite case.

Additionally, Fig. 7(a) shows the Cooper-pair-splitting efficiency as a function of the distance along the F/S interface for various M values. As can be seen, the efficiency becomes increasingly chiral as the magnetization increases at the same time as its maximum value in the range $0 < d < \xi_0$ gradually increases from 0.5 to $\sim$0.8. Figure 7(b) further reveals that efficiency rapidly reaches its peak for magnetization values on the order of Δ_0. Beyond this point, it remains constant for both s-wave and $d_{x^2-y^2}$ symmetries.

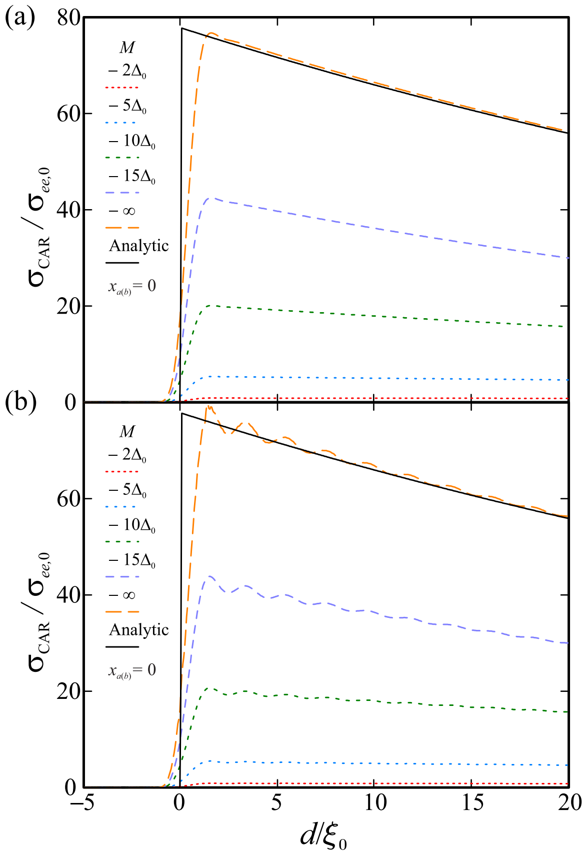

FIG. 6. Crossed Andreev reflection conductance $\sigma_{\rm CAR}(V=0)$ in the tunnel limit (a) for s-wave symmetry and (b) for $d_{x^2-y^2}$ and different values of magnetization ($E_{FR} = 13\ \Delta_0$, $\varepsilon = 0.002\ \Delta_0$). All curves are normalized as in Fig. 3(b).

Finally, Fig. 8 shows the effect of the transparency of the coupling between the normal electrodes and the F/S junction (see Appendix C). As can be seen in the plot, the normalized CAR conductance decreases globally and exhibits the characteristic behavior of the tunnel limit for values of the normalized hopping parameter $\tilde{t}_i$ less than 0.7. However, for higher values of $\tilde{t}_i$ approaching the transparent limit, the CAR conductance presents a minimum around $d \sim \xi_0$. This is associated with the momentary increase in the local Andreev reflections at the electrode point contacts. Despite this variation, the CAR conductance still preserves its long-range chiral character and efficiency above 0.58 for $d > 1.5\xi_0$, indicating that this behavior is independent of the contact barrier transparency.

V. CONCLUSIONS

We examined the efficiency of crossed Andreev reflection processes in a Cooper pair splitter device composed of two thin metal electrodes in contact with an F/S junction formed on the surface of a TI through the proximity effect. We considered a magnetization vector normal to the TI surface for the F region and an induced s- and d-wave superconducting order parameter for the S region. The compelling spinless chiral p-wave symmetry at the F/S interface presents chiral Majorana edge states. The chirality of these states can be

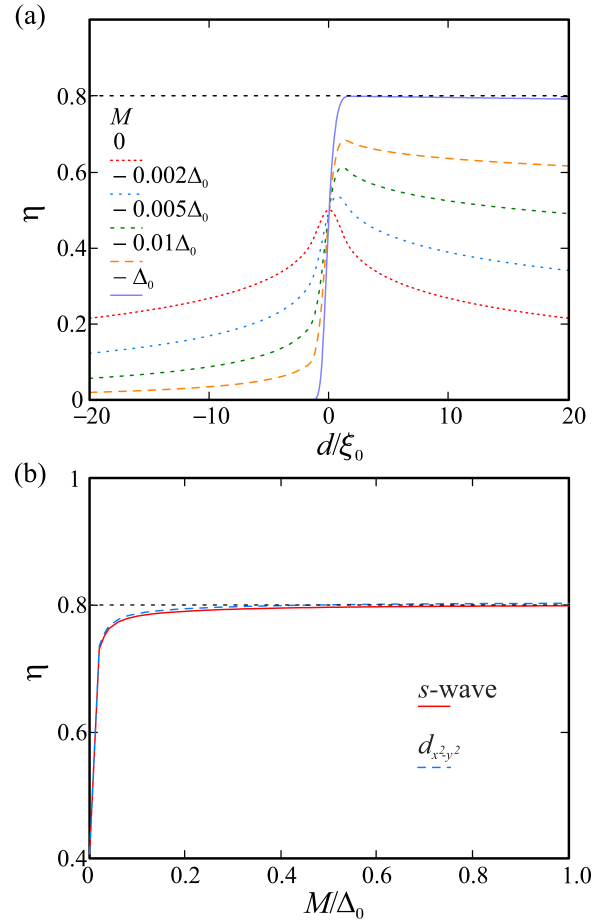

FIG. 7. Cooper-pair-splitting efficiency η as a function of (a) the electrode separation d for s-wave symmetry and different values of M and (b) magnetization for both s- and d-wave symmetries with $d = 1.6\xi_0$.

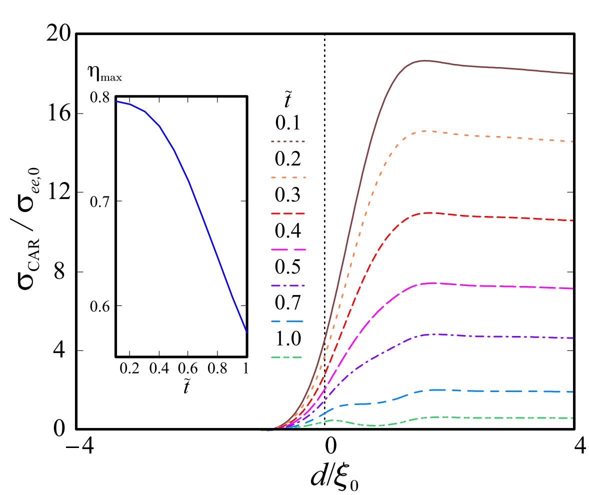

FIG. 8. Crossed Andreev reflection conductance $\sigma_{\rm CAR}(V=0)$ for s-wave symmetry, with $M = -10\Delta_0$ and different values of the normalized hopping amplitude $\tilde{t}$ ($\varepsilon = 0.002\ \Delta_0$). The inset shows the dependence of the maximum efficiency $\eta_{\max}$ for different values of $\tilde{t}$. All curves are normalized as in Fig. 3(b).

controlled by the magnetization polarization. Using a simple analytical model, we demonstrated that the conductance of crossed Andreev reflection mediated by chiral Majorana edge states along the F/S interface does not oscillate with electrode separation and exhibits slow decay in low-disorder samples (long-range behavior). Under a symmetrical voltage configuration, our system achieved a maximum splitting efficiency of 80% and remained stable with electrode separation for $M \sim \Delta_0$. Our results are also valid for the $d_{x^2-y^2}$ symmetry and could easily be extrapolated to finite temperatures, paving the way for potential experimental realization in high-T_c superconductors.

ACKNOWLEDGMENT

We wish to acknowledge the support of Universidad Nacional de Colombia, DIEB, Código Hermes 57739.

APPENDIX A: HAMILTONIAN APPROACH AND CALCULATION OF THE NONLOCAL CURRENT OF THE SYSTEM

For a superconducting system with two contacts (as in a Cooper pair splitter device), the Hamiltonian has the form [91,92,95,97]

$$\hat{H} = \hat{H}_a + \hat{H}_b + \hat{H}_s + \hat{H}_{as} + \hat{H}_{bs}, \tag{A1}$$

with $\hat{H}_{a,b,s}$ being the Hamiltonians of normal electrodes a and b and the superconducting region s and $\hat{H}_{is}$ being the hopping Hamiltonians between the point electrode i and region s,

$$\hat{H}_{is} = t_i \sum_{\sigma,\sigma'} e^{i\phi_i(\tau)/2} \hat{c}^\dagger_{i\sigma} \hat{b}_{i\sigma'} + \text{H.c.}, \tag{A2}$$

where $\sigma, \sigma' = \uparrow, \downarrow$ are the spin projection indices in the z direction and $\phi_i(\tau) = \phi_0 + 2(E_{F,i} - E_{F,s})\tau/\hbar$ are the time-dependent gauge phases induced by the gradient of the chemical potential in the vicinity of electrode $i = a, b$ with region S. Here, t_i is the hopping amplitude at this contact point, $\hat{c}_{i\sigma}$ are the annihilation operators for electrode i, and $\hat{b}_{i\sigma}$ are the annihilation operators at the point of region S in contact with electrode i. In the Heisenberg picture the average current in contact i is given by

$$\begin{aligned} I_i(\tau) &= -e\left\langle \frac{d}{d\tau} \hat{N}_i(\tau) \right\rangle \\ &= it_i \frac{e}{\hbar} \sum_{\sigma,\sigma'} [\langle \hat{c}^\dagger_{i\sigma}(\tau) \hat{b}_{i\sigma'}(\tau)\rangle - \langle \hat{b}^\dagger_{i\sigma'}(\tau) \hat{c}_{i\sigma}(\tau)\rangle], \end{aligned} \tag{A3}$$

which can be expressed in terms of the Keldysh Green's functions as

$$\hat{G}^{\alpha\beta}_{ijkl}(\tau_\alpha, \tau'_\beta) = -i\langle \hat{T}_c[\hat{D}_{q,ki}(\tau_\alpha) \hat{D}^\dagger_{q,lj}(\tau'_\beta)]\rangle, \tag{A4}$$

$$\hat{D}_{ki}(\tau) = (\hat{d}_{ki\uparrow}(\tau), \hat{d}_{ki\downarrow}(\tau), \hat{d}^\dagger_{ki\uparrow}(\tau), \hat{d}^\dagger_{ki\downarrow}(\tau))^T, \tag{A5}$$

with $i, j = a, b$ representing the contact indices, $k, l = N, S$ being the region indices ($\hat{d}_{ni\sigma} = \hat{c}_{i\sigma}, \hat{d}_{si\sigma} = \hat{b}_{i\sigma}$), $\alpha, \beta = +, -$ being the indices of the Keldysh temporal contour, and $\hat{T}_c$ being the Keldysh temporal ordering operator. Assuming normal electrodes on the surface of the TI, the hopping Hamiltonian (A2) takes the form of (B8). Considering the two possible choices of boundary conditions, the average current acquires a factor of 2 [73,97]. In a stationary situation, the average current in electrode i can be expressed in the energy space as

$$I_i = \frac{e}{h} \int dE \,\text{Tr}(\hat{\tau}_z[\hat{t}_i \hat{G}^{+-}_{iSN}(E) - \hat{t}^\dagger_i \hat{G}^{+-}_{iNS}(E)]), \tag{A6}$$

with $\hat{\tau}_k$ representing the Pauli matrices in Nambu space and $\hat{t}_i$ being the self-energy matrix associated with (A2); we employ shorthand notation for repeated indices ($ii \to i$). Using the Dyson equations [92]

$$\hat{G}^{+-}_{iSN}(E) = \hat{G}^{+-}_{iS}(E) \hat{t}^T_i \hat{g}^a_{iN}(E) + \hat{G}^r_{iS}(E) \hat{t}^T_i \hat{g}^{+-}_{iN}(E), \tag{A7}$$

$$\hat{G}^{+-}_{iNS}(E) = \hat{g}^{+-}_{iN}(E) \hat{t}_i \hat{G}^a_{iS}(E) + \hat{g}^r_{iN}(E) \hat{t}_i \hat{G}^{+-}_{iS}(E), \tag{A8}$$

the average current can be written in terms of Green's functions evaluated over a single type of region as

$$\begin{aligned} I_i = \frac{e}{2h} \int dE \,\text{Tr}\{\hat{\tau}_z \hat{t}^\dagger_i [&\hat{g}^{+-}_{iN}(E) \hat{t}_i \hat{G}^{-+}_{iS}(E) \\ &- \hat{g}^{-+}_{iN}(E) \hat{t}_i \hat{G}^{+-}_{iS}(E)]\}, \end{aligned} \tag{A9}$$

where the unperturbed Keldysh Green's functions of the electrodes are given by

$$\hat{g}^{+-}_{iN}(E) = 2\pi i \hat{\rho}_{iN}(E) \hat{n}_{iN}(E), \tag{A10}$$

$$\hat{g}^{-+}_{iN}(E) = -2\pi i \hat{\rho}_{iN}(E)[\hat{\tau}_0 \otimes \hat{\sigma}_0 - \hat{n}_{iN}(E)], \tag{A11}$$

with $\hat{n}_{iN}(E) = \text{diag}(n_{i,e\uparrow}(E), n_{i,e\downarrow}(E), n_{i,h\uparrow}(E), n_{i,h\downarrow}(E))$ being the occupation matrix of electrode i.

By considering the following Dyson equation, the nonequilibrium Green's functions can be expressed in terms of the local and nonlocal equilibrium Green's functions of the system ($\gamma = +-, -+$) [73,97]:

$$\hat{G}^\gamma_{iS} = \hat{G}^r_{iS} \hat{t}^\dagger_i \hat{g}^\gamma_{iN} \hat{t}_i \hat{G}^a_{iS} + \hat{G}^r_{ijS} \hat{t}_i \hat{g}^\gamma_{jS} \hat{t}^\dagger_i \hat{G}^a_{jiS}, \tag{A12}$$

which in turn are obtained from the equilibrium Green's function of the isolated regions $\hat{g}^{r/a}_{ijk}$ by a Dyson equation of the form

$$\hat{G}^{r/a}_{ijk} = \hat{g}^{r/a}_{ijk} + \hat{g}^{r/a}_{imk} \hat{\Sigma}_{mn} \hat{G}^{r/a}_{njk}, \tag{A13}$$

where the coupling self-energies between regions $\hat{\Sigma}_{mn} = \hat{\Sigma}^T_{nm} \equiv \hat{t}$ ($m, n = L, S$) correspond to the matrix form of $\hat{H}_{is}$. By defining the expression

$$I_{ij} = \frac{e}{h} \int dE \,\text{Tr}\tau_z \bar{\rho}_{iN} \left[\hat{n}_{iN} \hat{G}^r_{ijS} \bar{\rho}_{jN} - \hat{G}^r_{ijS} \bar{\rho}_{jN} \hat{n}_{jN}\right] \hat{G}^a_{ijS}, \tag{A14}$$

the total average current induced in electrode i takes the form

$$I_i = I_{ii} + I_{ij}, \tag{A15}$$

with $j \neq i$. Expressing (A14) in terms of matrices in the Nambu subspace we obtain expressions (4), (6), and (3) for a symmetrical voltage configuration. For independent (or different) voltages, I_{ij} presents an EC contribution given by

$$I_{\mathrm{EC}} = \frac{2e}{h}\int T_{\mathrm{EC},ij}(E)(n_{iN,e} - n_{jN,e})dE, \tag{A16}$$

$$T_{\mathrm{EC},ij}(E) = \mathrm{Tr}\big(\hat{\Gamma}_{iN,e}\hat{G}^{r}_{ijS,ee}\hat{\Gamma}_{jN,e}\hat{G}^{a}_{jiS,ee}\big). \tag{A17}$$

APPENDIX B: ASYMPTOTIC SOLUTION METHOD FOR GREEN'S FUNCTIONS IN TIs [73]

For a region in a planar junction with translational invariance along the y axis, the advanced (a) and retarded (r) Green's functions can be expressed as

$$\hat{g}^{r,a}(E,x,x',y-y') = \int dq\, \mathrm{e}^{iq(y-y')}\hat{g}^{r,a}(E,x,x',q), \tag{B1}$$

where the integrand satisfies the inhomogeneous equation

$$[(E \pm i\varepsilon) - \hat{H}(x,q)]\hat{g}^{r/a}(E,x,x',q) = \delta(x-x'), \tag{B2}$$

with E being the excitation energy of the system, q being the conserved wave vector along the interface, and ε being an infinitesimal scalar. These Green's functions can be expressed in terms of the asymptotic solutions of the system as

$$\hat{g}(x,x') = \begin{cases} \sum_{\mu,\nu=e,h}\hat{C}_{\mu\nu}\hat{\Psi}^{\mu}_{<}(x)\hat{\Psi}^{\nu T}_{>}(x') & x < x', \\ \sum_{\mu,\nu=e,h}\hat{C}'_{\mu\nu}\hat{\Psi}^{\nu}_{>}(x)\hat{\Psi}^{\mu T}_{<}(x') & x > x', \end{cases} \tag{B3}$$

where $\hat{C}_{\mu\nu}$ ($\nu = e, h$) are matrix coefficients determined by Eq. (B2) and $\hat{\Psi}^{\mu}_{<,>}(x)$ represent the asymptotic solutions of $\hat{H}$. These solutions obey specific boundary conditions at the left ($<$) and right ($>$) edges of region i. For the right semi-infinite superconducting region S, these solutions involve processes as conventional reflections ($\mu = \nu$) and branch exchange $e - h$ ($\mu \neq \nu$) at the interface:

$$\hat{\Psi}^{e}_{<}(x) = \hat{\psi}^{e}_{-}(x) + r^{ee}_{L}\hat{\psi}^{e}_{+}(x) + r^{eh}_{L}\hat{\psi}^{h}_{-}(x), \tag{B4}$$

$$\begin{aligned}\hat{\Psi}^{h}_{<}(x) &= \hat{\psi}^{h}_{+}(x) + r^{hh}_{L}\hat{\psi}^{h}_{-}(x) + r^{he}_{L}\hat{\psi}^{e}_{+}(x),\\ \hat{\Psi}^{e}_{>}(x) &= \hat{\psi}^{e}_{+}(x),\ \hat{\Psi}^{h}_{>}(x) = \hat{\psi}^{h}_{-}(x),\end{aligned} \tag{B5}$$

where $\hat{\psi}^{\mu}_{h}(x)$ are eigensolutions of $\hat{H}_{\mathrm{BdG}}(x,q)$ that propagate in the $\eta\hat{\mathbf{x}}$ ($h = \pm 1$) direction and $r^{\mu\nu}_{i}$ are the reflection coefficients on the left (L) or right (R) edge defined by the chosen boundary conditions. For the left magnetic normal region F, there are no $e - h$ conversion processes ($r^{eh}_{R} = r^{he}_{R} = 0$):

$$\hat{\Psi}^{e}_{>}(x) = \hat{\psi}^{e}_{+}(x) + r^{ee}_{R}\hat{\psi}^{e}_{-}(x), \tag{B6}$$

$$\begin{aligned}\hat{\Psi}^{h}_{>}(x) &= \hat{\psi}^{h}_{-}(x) + r^{hh}_{R}\hat{\psi}^{h}_{+}(x),\\ \hat{\Psi}^{e}_{<}(x) &= \hat{\psi}^{e}_{-}(x),\ \hat{\Psi}^{h}_{<}(x) = \hat{\psi}^{h}_{+}(x).\end{aligned} \tag{B7}$$

The surface of a TI lacks open boundaries, allowing for the selection of artificial boundary conditions as long as the corresponding $\hat{H}_T$ ensures a transparent coupling between the regions on the TI surface. In this work, we adopt the boundary conditions $\hat{\Psi}^{\mu}_{<,\downarrow}(x_L) = \hat{\Psi}^{\mu}_{>,\uparrow}(x_R) = 0$ for the spin components of spinors at the left x_L and right x_R edge of each region. Consequently, the coupling Hamiltonian $\hat{H}_T$ assumes the specific form

$$\hat{H}_T = t\int \mathrm{d}q\,\hat{c}^{\dagger}_{q,L\downarrow}\hat{c}_{q,R\uparrow} + \mathrm{H.c.}, \tag{B8}$$

with $t = \hbar v_F$ being the transparent hopping amplitude between adjacent regions. Thus, the equilibrium Green's functions of the coupled system $\hat{G}_{kl} = \hat{G}^{r/a}(x_k, x'_l)$ (x_k in region k) can be determined by a Dyson equation of the form of (A13):

$$\hat{G}_{kl} = \hat{g}_k\delta_{kl} + \hat{g}_k\delta_{km}\hat{\Sigma}_{mn}\hat{G}_{nl}, \tag{B9}$$

where the self-energies $\hat{\Sigma}_{LR} = \hat{\Sigma}^{T}_{RL} = t\tau_z(\sigma_x - i\sigma_y) \equiv \hat{t}$ correspond to the matrix form of $\hat{H}_T$. This boundary condition corresponds physically to a high-intensity magnetic barrier ($M \to \pm\infty$), where the spinor components with spin projection opposite to the magnetization direction become null. Therefore, to model large magnetization values and doping levels for the left region, it suffices to exclude the coupling with the F region and consider only the right semi-infinite region with an open boundary condition.

APPENDIX C: PARAMETERS OF THE MAGNETIC REGION'S GREEN'S FUNCTION

The spectrum of Hamiltonian (1) for the magnetic region in a TI surface is

$$E_{e/h} = \pm\left(\sqrt{(\hbar v_F|\mathbf{k}|)^2 + M^2} - E_F\right), \tag{C1}$$

with eigenspinors

$$\begin{aligned}\hat{\psi}^{e}_{\eta}(\mathbf{r}) &= \mathrm{e}^{iqy}\mathrm{e}^{\eta i k_e x}\big(\hat{\varphi}^{e}_{\varepsilon}, 0\big)^T,\\ \hat{\psi}^{h}_{\eta}(\mathbf{r}) &= \mathrm{e}^{iqy}\mathrm{e}^{\eta i k_h x}\big(0, \hat{\varphi}^{h}_{\varepsilon}\big)^T,\end{aligned} \tag{C2}$$

where

$$\hat{\varphi}^{e}_{\eta} = (M^{e}_{+}, -\eta i M^{e}_{-}\mathrm{e}^{\eta i\theta_e})^T/\sqrt{2}, \tag{C3}$$

$$\hat{\varphi}^{h}_{\eta} = (\eta i M^{h}_{+}\mathrm{e}^{\eta i\theta_h}, M^{h}_{-})^T/\sqrt{2}, \tag{C4}$$

$$M^{e}_{\pm} = \sqrt{E + E_F \pm M}/\sqrt{E + E_F}, \tag{C5}$$

$$M^{h}_{\pm} = \sqrt{E_F - E \pm M}/\sqrt{E_F - E}, \tag{C6}$$

$$\mathrm{e}^{i\theta_\mu} \equiv \hbar v_F(k_\mu + iq)/|\mathbf{k}|, \tag{C7}$$

and with the wave vector in the x direction,

$$k_{e/h} = \mathrm{sgn}(E_F \pm E)\sqrt{\frac{(E_F \pm E)^2 - M^2}{(\hbar v_F)^2} - q^2}, \tag{C8}$$

where sgn sets the correct sign for the valence band. For the chosen boundary conditions, the reflection coefficients are

$$r^{ee}_{R} = -1, \quad r^{hh}_{R} = \mathrm{e}^{-2i\theta_h}. \tag{C9}$$

Integrating Eq. (B2) between $x' - 0^+$ and $x' + 0^+$, we get the following constraint relation:

$$\hat{g}(x' + 0^+, x') - \hat{g}(x' - 0^+, x') = \frac{i}{\hbar v_F}(\tau_z \otimes \sigma_y). \tag{C10}$$

From this expression, we obtain the matrix coefficients of (B3) for this region:

$$\hat{C}_{\mu\nu} = \hat{C}_{\mu\mu}\delta_{\mu\nu}, \quad \hat{C}_{\mu\mu} = \hat{C}'_{\mu\mu} = \hat{C}_{ee}, \tag{C11}$$

$$\hat{C}_{ee} = \frac{-i}{\hbar v_F}\left(\frac{N_e}{\cos\theta_e}\frac{\tau_0+\tau_z}{2} + \frac{N_h}{\cos\theta_h}\frac{\tau_0-\tau_z}{2}\right), \quad \text{(C12)}$$

$$N_{e/h} = \frac{E_F \pm E}{\sqrt{(E_F\pm E)^2 - M^2}}. \quad \text{(C13)}$$

For the studied system, the contact points of the electrodes with the F region are modeled as heavily doped magnetic leads,

$$\hat{g}_i^{r(a)} \simeq \frac{-i}{\hbar v_F}\begin{pmatrix}\tilde{g} & 0\\ 0 & -\tilde{g}^*\end{pmatrix}, \quad \tilde{g} = \begin{pmatrix}0 & 1\\ 0 & i\end{pmatrix}. \quad \text{(C14)}$$

The effect of finite width L of the electrodes is modeled by a weight factor $f(q)$ in the Fourier transform (B1) of the equilibrium Green's functions of the junction [98,99],

$$\hat{G}_{ij}^{r,a}(E) \to \int dq\, |f(q)|^2 e^{iq(y_j-y_i)}\hat{G}^{r,a}(E, x_j, x_i, q), \quad \text{(C15)}$$

$$f(q) = \langle k_1|q\rangle\sqrt{k_F^2 - q^2}, \quad \text{(C16)}$$

$$\langle k_1|q\rangle = \sqrt{\frac{\pi}{L_y^3}}\frac{\cos(qL/2)}{k_1^2-q^2}. \quad \text{(C17)}$$

This factor is proportional to the transverse wave vector of states at the superconducting region and depends only on the first transverse mode of the electrode. ($k_1 = \pi/L$). The normalized hopping parameter $\tilde{t}$ between electrodes and the F/S region is related to this factor by the expression $\tilde{t} = t\sqrt{F_0}/\hbar v_F$, with

$$F_0 = \int dq |f(q)|^2. \quad \text{(C18)}$$

APPENDIX D: PARAMETERS OF THE SUPERCONDUCTING REGION'S GREEN'S FUNCTION

The excitation spectrum of Hamiltonian (1) for the superconducting region is

$$E(\mathbf{k}) = \sqrt{(\hbar v_F|\mathbf{k}| - E_F)^2 + |\hat{\Delta}|^2}, \quad \text{(D1)}$$

where $|\hat{\Delta}| = \mathrm{Tr}(\hat{\Delta}^\dagger\hat{\Delta})/2$ [100]. The associated eigenspinors are given by

$$\hat{\psi}_\eta^e(x) = e^{\eta i k_e x}\left(u_0\hat{\varphi}_\eta^e, -iv_0 e^{-i\phi_\eta}\sigma_y\hat{\varphi}_\eta^e\right)^T,$$
$$\hat{\psi}_\eta^h(x) = e^{\eta i k_h x}\left(-iv_0\sigma_y\hat{\varphi}_\eta^h, u_0\, e^{-i\phi_\eta}\hat{\varphi}_\eta^h\right)^T, \quad \text{(D2)}$$

where the coherence factors are defined as

$$u_0 = \sqrt{\frac{1}{2}\left(1+\frac{\Omega}{E}\right)},$$
$$v_0 = \sqrt{\frac{1}{2}\left(1-\frac{\Omega}{E}\right)}, \quad \text{(D3)}$$
$$\Omega = \sqrt{E^2 - |\Delta|^2}$$

and the spinors $\hat{\varphi}_\eta^\mu$ ($\mu = e, h$) are defined by the expressions

$$\hat{\varphi}_\eta^e = \left(1, -\eta i e^{\eta i\theta_e}\right)^T/\sqrt{2}, \quad \text{(D4)}$$

$$\hat{\varphi}_\eta^h = \left(\eta i e^{\eta i\theta_h}, 1\right)^T/\sqrt{2}, \quad \text{(D5)}$$

with the wave vector in the x direction

$$k_{e/h} = \sqrt{\frac{(E_F\pm\Omega)^2}{\hbar^2 v_F^2} - q^2}. \quad \text{(D6)}$$

For the chosen boundary conditions, the reflection coefficients are

$$\begin{aligned}
r_L^{ee} &= \frac{1}{Y}\left(e^{-i\theta_e} - \gamma_0^2 e^{-i\theta_h}\right)e^{-i\phi_-},\\
r_L^{eh} &= -\frac{1}{Y}\gamma_0\left(e^{-i\theta_e}e^{-i\phi_+} + e^{i\theta_e}e^{-i\phi_-}\right),\\
r_L^{he} &= -\frac{1}{Y}\gamma_0\left(e^{-i\theta_h}e^{-i\phi_+} + e^{i\theta_h}e^{-i\phi_-}\right),\\
r_L^{hh} &= -\frac{1}{Y}\left(e^{i\theta_e} - \gamma_0^2 e^{i\theta_h}\right)e^{-i\phi_+},\\
Y &= \gamma_0^2 e^{-i\theta_h}e^{-i\phi_+} + e^{i\theta_e}e^{-i\phi_-}, \quad \gamma_0 = v_0/u_0.
\end{aligned}$$

In this case the matrix coefficients of (B3) are given by

$$\hat{C}_{ee} = -\frac{1}{\hbar v}\frac{1}{C^2+BF-AH}\begin{pmatrix} H & 0 & -C & B\\ 0 & H & -F & -C\\ C & B & -A & 0\\ -F & C & 0 & -A\end{pmatrix},$$

$$\hat{C}_{hh} = \Lambda\hat{C}_{ee},\ \hat{C}_{eh} = \hat{C}_{he} = 0,$$

where

$$\begin{aligned}
A &= i(e^{-i\theta_e} + e^{i\theta_e}) - \Lambda i\gamma_0^2(e^{-i\theta_h} + e^{i\theta_h}),\\
B &= i\gamma_0\Lambda(e^{i\theta_h}e^{-i\phi_+} + e^{-i\theta_h}e^{-i\phi_-})\\
&\quad - i\gamma_0(e^{i\theta_e}e^{-i\phi_+} + e^{-i\theta_e}e^{-i\phi_-}),\\
C &= \gamma_0(e^{-i\phi_+} - e^{-i\phi_-})(\Lambda - 1),\\
F &= i\gamma_0\Lambda(e^{-i\theta_h}e^{-i\phi_+} + e^{i\theta_h}e^{-i\phi_-})\\
&\quad - i\gamma_0(e^{-i\theta_e}e^{-i\phi_+} + e^{i\theta_e}e^{-i\phi_-}),\\
H &= i\gamma_0^2(e^{-i\theta_e} + e^{i\theta_e})e^{-i\phi_+}e^{-i\phi_-}\\
&\quad - \Lambda i(e^{-i\theta_h} + e^{i\theta_h})e^{-i\phi_+}e^{-i\phi_-},\\
\Lambda &= r_L^{eh}/r_L^{he}.
\end{aligned}$$

APPENDIX E: CAR PROCESSES IN CONVENTIONAL CHIRAL *p*-WAVE SUPERCONDUCTIVITY

For a conventional superconductor, the element eh of the Green's function evaluated at the edge of a semi-infinite region is given by

$$\hat{g}_{S0,eh}^{r,a}(E,q) = \frac{-2im}{\hbar^2 D}\gamma_0 e^{i\varphi_-} \quad \text{(E1)}$$
$$\times\left[\frac{1}{k_e} + \frac{1}{k_h} + \frac{D(1-e^{i\Delta\varphi})}{2(1-\gamma^2)}\left(\frac{1}{k_e} - \frac{1}{k_h}\right)\right], \quad \text{(E2)}$$

$$D = \left(1 - \gamma_0^2 e^{-i\Delta\varphi}\right), \quad \text{(E3)}$$

with m being the mass of the electron. For chiral p-wave symmetry $\Delta(\theta) = \Delta_0 e^{i\theta}$, and then $e^{i\varphi_+} = e^{i\theta} = -e^{-i\varphi_-}$, and for $E = 0 + i\varepsilon$ and $E_F \gg \Delta_0$ ($k_e \approx k_h$) we get

$$\hat{g}^{r,a}_{S0,eh}(0,\theta) \approx -\frac{4m}{\hbar^2}\frac{\delta e^{-i\theta}}{(1-\delta^2 e^{-2i\theta})}\frac{1}{k_F\cos\theta},$$
$$\delta = \sqrt{\frac{\zeta-\varepsilon}{\zeta+\varepsilon}}, \quad \zeta = \sqrt{\varepsilon^2+\Delta_0^2}. \tag{E4}$$

Expressing the corresponding integral (C15) in terms of $q \approx k_F \sin\theta$, we obtain for (8)

$$\sigma_{\mathrm{CAR}}(d) = \sigma_0\tilde{\Gamma}_{e,b}\tilde{\Gamma}_{h,a}\left(\frac{4mL}{\hbar^2}\right)^2\left(\frac{k_F}{\pi}\right)^4\Theta^2(sd)e^{-d/\lambda}, \tag{E5}$$

which has a dependence on the electrode separation d identical to that of the case studied above for a TI in contact with a conventional s-wave superconductor.

[1] G. Burkard, Spin-entangled electrons in solid-state systems, J. Phys.: Condens. Matter **19**, 233202 (2007).
[2] J. M. Byers and M. E. Flatté, Probing spatial correlations with nanoscale two-contact tunneling, Phys. Rev. Lett. **74**, 306 (1995).
[3] G. Deutscher and D. Feinberg, Coupling superconducting-ferromagnetic point contacts by Andreev reflections, Appl. Phys. Lett. **76**, 487 (2000).
[4] G. Falci, D. Feinberg, and F. W. J. Hekking, Correlated tunneling into a superconductor in a multiprobe hybrid structure, Europhys. Lett. **54**, 255 (2001).
[5] G. B. Lesovik, T. Martin, and G. Blatter, Electronic entanglement in the vicinity of a superconductor, Eur. Phys. J. B **24**, 287 (2001).
[6] N. M. Chtchelkatchev, G. Blatter, G. B. Lesovik, and T. Martin, Bell inequalities and entanglement in solid-state devices, Phys. Rev. B **66**, 161320(R) (2002).
[7] C. Bena, S. Vishveshwara, L. Balents, and M. P. A. Fisher, Quantum entanglement in carbon nanotubes, Phys. Rev. Lett. **89**, 037901(R) (2002).
[8] D. Feinberg, Andreev scattering and cotunneling between two superconductor-normal metal interfaces: The dirty limit, Eur. Phys. J. B **36**, 419 (2003).
[9] R. Mélin and S. Peysson, Crossed Andreev reflection at ferromagnetic domain walls, Phys. Rev. B **68**, 174515 (2003).
[10] T. Yamashita, S. Takahashi, and S. Maekawa, Crossed Andreev reflection in structures consisting of a superconductor with ferromagnetic leads, Phys. Rev. B **68**, 174504 (2003).
[11] N. Stefanakis and R. M. lin, Transport properties of ferromagnet-d-wave superconductor ferromagnet double junctions, J. Phys.: Condens. Matter **15**, 4239 (2003).
[12] R. Mélin and D. Feinberg, Sign of the crossed conductances at a ferromagnet/superconductor/ferromagnet double interface, Phys. Rev. B **70**, 174509 (2004).
[13] E. Prada and F. Sols, Entangled electron current through finite size normal-superconductor tunneling structures, Eur. Phys. J. B **40**, 379 (2004).
[14] D. Beckmann, H. B. Weber, and H. v. Löhneysen, Evidence for crossed Andreev reflection in superconductor-ferromagnet hybrid structures, Phys. Rev. Lett. **93**, 197003 (2004).
[15] S. Russo, M. Kroug, T. M. Klapwijk, and A. F. Morpurgo, Experimental observation of bias-dependent nonlocal Andreev reflection, Phys. Rev. Lett. **95**, 027002 (2005).
[16] A. Brinkman and A. A. Golubov, Crossed Andreev reflection in diffusive contacts: Quasiclassical Keldysh-Usadel formalism, Phys. Rev. B **74**, 214512 (2006).
[17] P. Cadden-Zimansky and V. Chandrasekhar, Nonlocal correlations in normal-metal superconducting systems, Phys. Rev. Lett. **97**, 237003 (2006).
[18] A. L. Yeyati, F. S. Bergeret, A. Martín-Rodero, and T. M. Klapwijk, Entangled Andreev pairs and collective excitations in nanoscale superconductors, Nat. Phys. **3**, 455 (2007).
[19] D. Beckmann and H. v. Löhneysen, Negative four-terminal resistance as a probe of crossed Andreev reflection, Appl. Phys. A **89**, 603 (2007).
[20] M. S. Kalenkov and A. D. Zaikin, Nonlocal Andreev reflection at high transmissions, Phys. Rev. B **75**, 172503 (2007).
[21] M. S. Kalenkov and A. D. Zaikin, Crossed Andreev reflection at spin-active interfaces, Phys. Rev. B **76**, 224506 (2007).
[22] C. Benjamin and J. K. Pachos, Detecting entangled states in graphene via crossed Andreev reflection, Phys. Rev. B **78**, 235403 (2008).
[23] D. S. Golubev, M. S. Kalenkov, and A. D. Zaikin, Crossed Andreev reflection and charge imbalance in diffusive normal-superconducting-normal structures, Phys. Rev. Lett. **103**, 067006 (2009).
[24] P. Cadden-Zimansky, J. Wei, and V. Chandrasekhar, Cooper-pair-mediated coherence between two normal metals, Nat. Phys. **5**, 393 (2009).
[25] H. Haugen, D. Huertas-Hernando, A. Brataas, and X. Waintal, Crossed Andreev reflection versus electron transfer in three-terminal graphene devices, Phys. Rev. B **81**, 174523 (2010).
[26] P. Burset, W. J. Herrera, and A. L. Yeyati, Microscopic theory of Cooper pair beam splitters based on carbon nanotubes, Phys. Rev. B **84**, 115448 (2011).
[27] S. Gómez, P. Burset, W. J. Herrera, and A. L. Yeyati, Selective focusing of electrons and holes in a graphene-based superconducting lens, Phys. Rev. B **85**, 115411 (2012).
[28] R. Beiranvand, H. Hamzehpour, and M. Alidoust, Nonlocal Andreev entanglements and triplet correlations in graphene with spin-orbit coupling, Phys. Rev. B **96**, 161403(R) (2017).
[29] M. Beconcini, M. Polini, and F. Taddei, Nonlocal superconducting correlations in graphene in the quantum Hall regime, Phys. Rev. B **97**, 201403(R) (2018).
[30] D. S. Golubev and A. D. Zaikin, Cross-correlated shot noise in three-terminal superconducting hybrid nanostructures, Phys. Rev. B **99**, 144504 (2019).
[31] X. Wu, H. Meng, F. Kong, H. Zhang, Y. Bai, and N. Xu, Tunable nonlocal valley-entangled Cooper pair splitter realized in bilayer-graphene van der Waals spin valves, Phys. Rev. B **101**, 125406 (2020).

[32] M. F. Jakobsen, A. Brataas, and A. Qaiumzadeh, Electrically controlled crossed Andreev reflection in two-dimensional antiferromagnets, Phys. Rev. Lett. **127**, 017701 (2021).

[33] P. Recher, E. V. Sukhorukov, and D. Loss, Andreev tunneling, Coulomb blockade, and resonant transport of nonlocal spin-entangled electrons, Phys. Rev. B **63**, 165314 (2001).

[34] P. Recher and D. Loss, Dynamical Coulomb blockade and spin-entangled electrons, Phys. Rev. Lett. **91**, 267003 (2003).

[35] L. Hofstetter, S. Csonka, J. Nygård, and C. Schönenberger, Cooper pair splitter realized in a two-quantum-dot y-junction, Nature (London) **461**, 960 (2009).

[36] L. G. Herrmann, F. Portier, P. Roche, A. L. Yeyati, T. Kontos, and C. Strunk, Carbon nanotubes as Cooper-pair beam splitters, Phys. Rev. Lett. **104**, 026801 (2010).

[37] J. Schindele, A. Baumgartner, and C. Schönenberger, Near-unity Cooper pair splitting efficiency, Phys. Rev. Lett. **109**, 157002 (2012).

[38] A. Cottet, T. Kontos, and A. L. Yeyati, Subradiant split Cooper pairs, Phys. Rev. Lett. **108**, 166803 (2012).

[39] G. Michałek, B. R. Bułka, T. Domański, and K. I. Wysokiński, Interplay between direct and crossed Andreev reflections in hybrid nanostructures, Phys. Rev. B **88**, 155425 (2013).

[40] G. Michałek, T. Domański, B. R. Bułka, and K. I. Wysokiński, Novel non-local effects in three-terminal hybrid devices with quantum dot, Sci. Rep. **5**, 14572 (2015).

[41] G. Michałek, T. Domanski, and K. Wysokinski, Cooper pair splitting efficiency in the hybrid three-terminal quantum dot, J. Supercond. Novel Magn. **30**, 135 (2017).

[42] K. Bocian, W. Rudziński, and I. Weymann, Splitting efficiency and interference effects in a Cooper pair splitter based on a triple quantum dot with ferromagnetic contacts, Phys. Rev. B **97**, 195441 (2018).

[43] S. Takahashi, T. Yamashita, and S. Maekawa, Quantum interference due to crossed Andreev reflection in a d-wave superconductor with two nano-contacts, J. Phys. Chem. Solids **67**, 325 (2006).

[44] P. Burset, W. Herrera, and A. Levy Yeyati, Proximity-induced interface bound states in superconductor-graphene junctions, Phys. Rev. B **80**, 041402(R) (2009).

[45] J. A. Celis Gil, S. Gomez P., and W. J. Herrera, Noise cross-correlation and Cooper pair splitting efficiency in multiteminal superconductor junctions, Solid State Commun. **258**, 25 (2017).

[46] Y.-T. Zhang, X. Deng, Q.-F. Sun, and Z. Qiao, High-efficiency Cooper-pair splitter in quantum anomalous Hall insulator proximity-coupled with superconductor, Sci. Rep. **5**, 14892 (2015).

[47] Z. Hou, Y. Xing, A.-M. Guo, and Q.-F. Sun, Crossed Andreev effects in two-dimensional quantum Hall systems, Phys. Rev. B **94**, 064516 (2016).

[48] G. E. Volovik, *The Universe in a Helium Droplet*, OUP International Series of Monographs on Physics (Clarendon, Oxford, 2003).

[49] G. E. Volovik, On edge states in superconductors with time inversion symmetry breaking, JETP Lett. **66**, 522 (1997).

[50] M. Z. Hasan and C. L. Kane, Colloquium: Topological insulators, Rev. Mod. Phys. **82**, 3045 (2010).

[51] X.-L. Qi and S.-C. Zhang, Topological insulators and superconductors, Rev. Mod. Phys. **83**, 1057 (2011).

[52] W. Huang, E. Taylor, and C. Kallin, Vanishing edge currents in non-*p*-wave topological chiral superconductors, Phys. Rev. B **90**, 224519 (2014).

[53] A. P. Schnyder and P. M. R. Brydon, Topological surface states in nodal superconductors, J. Phys.: Condens. Matter **27**, 243201 (2015).

[54] M. Sato and Y. Ando, Topological superconductors: A review, Rep. Prog. Phys. **80**, 076501 (2017).

[55] A. Haim and Y. Oreg, Time-reversal-invariant topological superconductivity in one and two dimensions, Phys. Rep. **825**, 1 (2019).

[56] F. Wilczek, Majorana returns, Nat. Phys. **5**, 614 (2009).

[57] J. Alicea, Y. Oreg, G. Refael, F. von Oppen, and M. P. A. Fisher, Non-Abelian statistics and topological quantum information processing in 1D wire networks, Nat. Phys. **7**, 412 (2011).

[58] J. K. Pachos, *Introduction to Topological Quantum Computation* (Cambridge University Press, Cambridge, 2012).

[59] S. R. Elliott and M. Franz, Colloquium: Majorana fermions in nuclear, particle, and solid-state physics, Rev. Mod. Phys. **87**, 137 (2015).

[60] C. Beenakker, Search for Majorana fermions in superconductors, Annu. Rev. Condens. Matter Phys. **4**, 113 (2013).

[61] S. D. Sarma, M. Freedman, and C. Nayak, Majorana zero modes and topological quantum computation, npj Quantum Inf. **1**, 15001 (2015).

[62] L. Fu and C. L. Kane, Superconducting proximity effect and Majorana fermions at the surface of a topological insulator, Phys. Rev. Lett. **100**, 096407 (2008).

[63] Y. Tanaka, T. Yokoyama, and N. Nagaosa, Manipulation of the Majorana fermion, Andreev reflection, and Josephson current on topological insulators, Phys. Rev. Lett. **103**, 107002 (2009).

[64] T. D. Stanescu, J. D. Sau, R. M. Lutchyn, and S. Das Sarma, Proximity effect at the superconductor–topological insulator interface, Phys. Rev. B **81**, 241310(R) (2010).

[65] J. Linder, Y. Tanaka, T. Yokoyama, A. Sudbø, and N. Nagaosa, Interplay between superconductivity and ferromagnetism on a topological insulator, Phys. Rev. B **81**, 184525 (2010).

[66] P. Zareapour, A. Hayat, S. Y. F. Zhao, M. Kreshchuk, A. Jain, D. C. Kwok, N. Lee, S.-W. Cheong, Z. Xu, A. Yang, G. D. Gu, S. Jia, R. J. Cava, and K. S. Burch, Proximity-induced high-temperature superconductivity in the topological insulators Bi_2Se_3 and Bi_2Te_3, Nat. Commun. **3**, 1056 (2012).

[67] G. Koren, T. Kirzhner, Y. Kalcheim, and O. Millo, Signature of proximity-induced $p_x + ip_y$ triplet pairing in the doped topological insulator Bi_2Se_3 by the s-wave superconductor NbN, Europhys. Lett. **103**, 67010 (2013).

[68] J.-P. Xu, M.-X. Wang, Z. L. Liu, J.-F. Ge, X. Yang, C. Liu, Z. A. Xu, D. Guan, C. L. Gao, D. Qian, Y. Liu, Q.-H. Wang, F.-C. Zhang, Q.-K. Xue, and J.-F. Jia, Experimental detection of a Majorana mode in the core of a magnetic vortex inside a topological insulator-superconductor $Bi_2Te_3/NbSe_2$ heterostructure, Phys. Rev. Lett. **114**, 017001 (2015).

[69] H.-H. Sun, K.-W. Zhang, L.-H. Hu, C. Li, G.-Y. Wang, H.-Y. Ma, Z.-A. Xu, C.-L. Gao, D.-D. Guan, Y.-Y. Li, C. Liu, D. Qian, Y. Zhou, L. Fu, S.-C. Li, F.-C. Zhang, and J.-F. Jia, Majorana zero mode detected with spin selective Andreev

reflection in the vortex of a topological superconductor, Phys. Rev. Lett. **116**, 257003 (2016).
[70] H.-H. Sun and J.-F. Jia, Detection of Majorana zero mode in the vortex, npj Quantum Mater. **2**, 34 (2017).
[71] W. Dai, A. Richardella, R. Du, W. Zhao, X. Liu, C. X. Liu, S.-H. Huang, R. Sankar, F. Chou, N. Samarth, and Q. Li, Proximity-effect-induced superconducting gap in topological surface states – A point contact spectroscopy study of $NbSe_2/Bi_2Se_2$ superconductor-topological insulator heterostructures, Sci. Rep. **7**, 7631 (2017).
[72] O. E. Casas, L. Arrachea, W. J. Herrera, and A. L. Yeyati, Proximity induced time-reversal topological superconductivity in Bi_2Se_3 films without phase tuning, Phys. Rev. B **99**, 161301(R) (2019).
[73] O. E. Casas, S. G. Páez, and W. J. Herrera, A Green's function approach to topological insulator junctions with magnetic and superconducting regions, J. Phys.: Condens. Matter **32**, 485302 (2020).
[74] Z. Zhu, M. Papaj, X.-A. Nie, H.-K. Xu, Y.-S. Gu, X. Yang, D. Guan, S. Wang, Y. Li, C. Liu, J. Luo, Z.-A. Xu, H. Zheng, L. Fu, and J.-F. Jia, Discovery of segmented Fermi surface induced by Cooper pair momentum, Science **374**, 1381 (2021).
[75] D. Kiphart, Y. Harkavyi, K. Balin, J. Szade, B. Mróz, P. Kuświk, S. Jurga, and M. Wiesner, Investigations of proximity-induced superconductivity in the topological insulator Bi_2Te_3 by microraman spectroscopy, Sci. Rep. **11**, 22980 (2021).
[76] M. Bai, X.-K. Wei, J. Feng, M. Luysberg, A. Bliesener, G. Lippertz, A. Uday, A. A. Taskin, J. Mayer, and Y. Ando, Proximity-induced superconductivity in $(Bi_{1-x}Sb_x)_2Te_3$ topological-insulator nanowires, Commun. Mater. **3**, 20 (2022).
[77] C. Li, Y.-F. Zhao, A. Vera, O. Lesser, H. Yi, S. Kumari, Z. Yan, C. Dong, T. Bowen, K. Wang, H. Wang, J. L. Thompson, K. Watanabe, T. Taniguchi, D. Reifsnyder Hickey, Y. Oreg, J. A. Robinson, C.-Z. Chang, and J. Zhu, Proximity-induced superconductivity in epitaxial topological insulator/graphene/gallium heterostructures, Nat. Mater. **22**, 570 (2023).
[78] Z. P. Niu, Crossed Andreev reflection on a topological insulator, J. Appl. Phys. **108**, 103904 (2010).
[79] R. Vali and H. F. Khouzestani, Nonlocal transport properties of topological insulator F/I/SC/I/F junction with perpendicular magnetization, Eur. Phys. J. B **87**, 25 (2014).
[80] R. Vali and H. Khouzestani, Crossed Andreev reflection in topological insulator F/d-wave SC/F junction, Phys. E (Amsterdam, Neth.) **68**, 107 (2015).
[81] S. K. Firoz Islam, P. Dutta, and A. Saha, Enhancement of crossed Andreev reflection in a normal-superconductor-normal junction made of thin topological insulator, Phys. Rev. B **96**, 155429 (2017).
[82] K. Zhang and Q. Cheng, Electrically tunable crossed Andreev reflection in a ferromagnet–superconductor–ferromagnet junction on a topological insulator, Supercond. Sci. Technol. **31**, 075001 (2018).
[83] S. Ikegaya, Y. Asano, and D. Manske, Anomalous nonlocal conductance as a fingerprint of chiral Majorana edge states, Phys. Rev. Lett. **123**, 207002 (2019).
[84] A. P. Mackenzie, R. K. W. Haselwimmer, A. W. Tyler, G. G. Lonzarich, Y. Mori, S. Nishizaki, and Y. Maeno, Extremely strong dependence of superconductivity on disorder in Sr_2RuO_4, Phys. Rev. Lett. **80**, 161 (1998).
[85] M. S. Anwar and J. W. A. Robinson, A review of electronic transport in superconducting Sr_2RuO_4 junctions, Coatings **11**, 1110 (2021).
[86] A. V. Balatsky, I. Vekhter, and J.-X. Zhu, Impurity-induced states in conventional and unconventional superconductors, Rev. Mod. Phys. **78**, 373 (2006).
[87] P. G. De Gennes, *Superconductivity of Metals and Alloys*, Advanced Book Classics (Perseus, Cambridge, MA, 1999).
[88] J.-X. Zhu, Transport across normal-metal/superconductor junctions, in *Bogoliubov-de Gennes Method and Its Applications* (Springer, Cham, 2016), pp. 141–167.
[89] H. Zhang, C.-X. Liu, X.-L. Qi, X. Dai, Z. Fang, and S.-C. Zhang, Topological insulators in Bi_2Se_3, Bi_2Te_3, and Sb_2Te_3 with a single Dirac cone on the surface, Nat. Phys. **5**, 438 (2009).
[90] P. G. Silvestrov, P. W. Brouwer, and E. G. Mishchenko, Spin and charge structure of the surface states in topological insulators, Phys. Rev. B **86**, 075302 (2012).
[91] J. C. Cuevas, A. Martín-Rodero, and A. Levy Yeyati, Hamiltonian approach to the transport properties of superconducting quantum point contacts, Phys. Rev. B **54**, 7366 (1996).
[92] J. C. Cuevas and E. Scheer, *Molecular Electronics: An Introduction to Theory and Experiment*, World Scientific Series in Nanoscience and Nanotechnology Vol. 1 (World Scientific, Singapore, 2010).
[93] W. L. McMillan, Theory of superconductor–normal-metal interfaces, Phys. Rev. **175**, 559 (1968).
[94] W. J. Herrera, P. Burset, and A. L. Yeyati, A Green function approach to graphene–superconductor junctions with well-defined edges, J. Phys.: Condens. Matter **22**, 275304 (2010).
[95] O. E. Casas, S. Gómez Páez, A. Levy Yeyati, P. Burset, and W. J. Herrera, Subgap states in two-dimensional spectroscopy of graphene-based superconducting hybrid junctions, Phys. Rev. B **99**, 144502 (2019).
[96] T. Löfwander, V. S. Shumeiko, and G. Wendin, Andreev bound states in high-T_c superconducting junctions, Supercond. Sci. Technol. **14**, R53 (2001).
[97] O. E. Casas, Transporte eléctrico en nanoestructuras topológicas, Ph.D. thesis, 2019, https://repositorio.unal.edu.co/handle/unal/76648.
[98] Y. Takagaki and K. H. Ploog, Quantum point contact spectroscopy of d-wave superconductors, Phys. Rev. B **60**, 9750 (1999).
[99] W. J. Herrera, A. Levy Yeyati, and A. Martín-Rodero, Long-range crossed Andreev reflections in high-temperature superconductors, Phys. Rev. B **79**, 014520 (2009).
[100] M. Sigrist, Introduction to unconventional superconductivity, AIP Conf. Proc. **789**, 165 (2005).